Outdoor to indoor office MIMO measurements at 5.2 GHz

Wyne, Shurjeel; Almers, Peter; Eriksson, Gunnar; Kåredal, Johan; Tufvesson, Fredrik; Molisch, Andreas

Link to publication

Outdoor to Indoor Office MIMO Measurements at 5.2 GHz

Shurjeel Wyne[1], Peter Almers[1,2], Gunnar Eriksson[1,3], Johan Karedal[1],
Fredrik Tufvesson[1], and Andreas F. Molisch[1,4]

[1]Dept. of Electroscience, Lund University, Box 118, SE-221 00 Lund, Sweden.

[2]TeliaSonera AB, Box 94, SE-201 20 Malmö, Sweden

[3]Swedish Defence Research Agency, Box 1165, SE-581 11 Linköping, Sweden

[4]Mitsubishi Electric Research Labs, 201 Broadway, Cambridge, MA 02139, USA

E-mail: Firstname.Lastname@es.lth.se

Abstract—**This paper presents the results of one of the first measurement campaigns for the double-directional characterization of outdoor to indoor wireless propagation channels. Such channels play a vital role for cellular systems with multiple antenna elements at transmitter and receiver, i.e. multiple-input multiple-output (MIMO) systems. Measurements were performed at 5.2 GHz between 53 different receiver locations in an office building, and three "base station" positions on a nearby rooftop. In the paper we present results for angular-delay profiles, RMS angular spread, and other statistical parameters characterizing delay and angular dispersion.**

I. INTRODUCTION

Under ideal circumstances, multiple antennas at both receiver and transmitter side can result in tremendous capacity improvements over single antenna systems [1]. However, the propagation channel between transmitter and receiver is an important limiting factor for the possible capacity gain. Understanding the MIMO channel is thus of great importance for investigating performance limits of MIMO systems, as well as designing systems that efficiently utilize this channel. Channel measurements are a vital prerequisite for such an understanding, as well as for the derivation of channel models that can be used for system design and simulation.

Two types of MIMO channel characterizations have evolved in the last 10 years: (i) the transfer function matrix **H**, whose entries are the transfer functions from each transmit antenna element to each receive antenna element, and (ii) a double-directional description of the channel, i.e., a description of the directions of the multipath components at both link ends [2]. The latter method is more general, as it is independent of the antenna patterns and array configurations, and will be the one used in this paper.

There are a number of double-directional outdoor to outdoor and indoor to indoor measurement results reported in the literature, e.g., [2], [3], [4], [5], [6], [7], [8]. However, there is a remarkable lack of outdoor to indoor measurement results. Only recently, in parallel to our work, Medbo et al. [9] and Nguyen et al. [10] have performed outdoor to indoor MIMO measurements. The outdoor to indoor scenario has important applications for

data transmission in third generation cellular systems, as well as wireless LANs.

In this paper we present the results of a double-directional MIMO channel measurement campaign, for an outdoor to indoor office scenario, carried out at 5.2 GHz. We analyze the direction-of-departure (DOD) and direction-of-arrival (DOA), as well as the distributions of root mean square (RMS) angular spreads and RMS delay spreads.

The paper is organized as follows: In Sec. II the measurement setup and scenario are described, Sec. III deals with data evaluation, results are presented in Sec. IV, and finally in Sec. V we summarize the results.

II. MEASUREMENT SETUP

A. Measurement equipment

Measurement data were recorded with the RUSK ATM channel sounder [5]. The measurements were performed at a center frequency of 5.2 GHz and a signal bandwidth of 120 MHz, and with a transmit power of 33 dBm. The receive antenna was a 16-element uniform circular array with vertically polarized monopole elements, with a radius of approximately one wavelength λ. The transmit antenna was an 8 element dual polarized uniform linear patch array with element spacing $\lambda/2$ (see Fig. 1). Only the 8 vertically polarized elements on the transmitter were considered for the DOA-DOD analysis. The transmitter emitted a signal that was periodically-repeated every 1.6 μs. At the receiver, the transfer function was measured at 193 points in the frequency domain, and stored. The sampling time for one MIMO snapshot was 819 μs, which is within the coherence time of the channel. 13 snapshots were measured at each receive location. The time between successive snapshots was 4.1 ms.

B. Measurement scenario

The measurement site is the "E-building" at LTH, Lund University, Sweden; a site map is shown in Fig. 2. 159 MIMO measurements were made from the roof of RF corridor (3rd floor) to offices in ASIC corridor (2nd floor). The transmitter was placed at three different positions on the roof. For each transmit position, the receiver was placed at 53 measurement positions spread
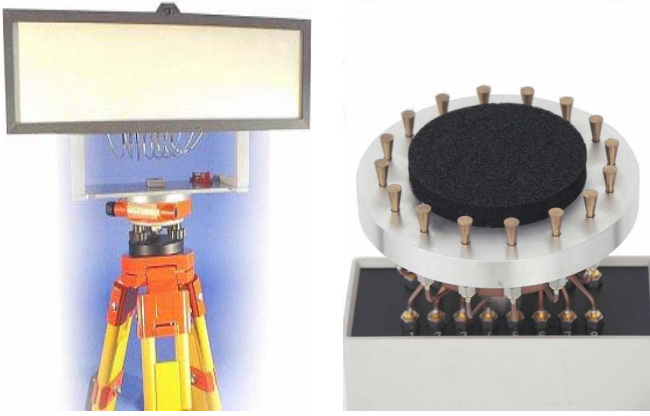
Fig. 1. An 8-element dual polarized uniform linear patch array was used at the transmitter side and a 16-element vertical polarized uniform circular array was used at the receiver side.
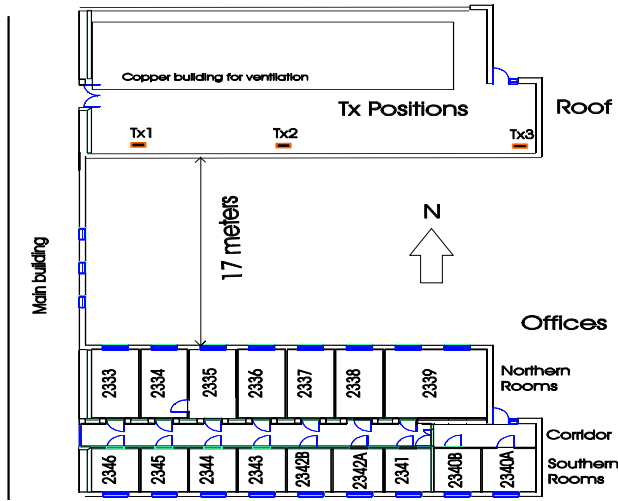

Fig. 2. Site map showing locations of Tx (3rd floor) and Rx positions (2nd floor). The distance between the blocks is also indicated. 4-7 positions were measured in room: 2334, 2336, 2337,2339 (referred to as north) and 2345, 2343, 2342A, 2340B (referred to as south).

over 8 different rooms and the corridor, see Fig. 5, thus a total of 159 measurements.

III. DATA EVALUATION

To jointly determine the DOA and DOD of the double directional channel, the high resolution SAGE algorithm [11] was used. The data evaluation is based on the assumption that the received and transmitted signals can be described as a finite number of plane waves:

$$h_{m,n}\left(k, i, \alpha_l, \tau_l, \phi_l^{\text{Rx}}, \phi_l^{\text{Tx}}, \nu_l\right) = \quad (1)$$

$$\sum_{l=1}^{L} \alpha_l e^{-j2\pi\Delta f \tau_l k} G_{\text{Tx}}\left(n, \phi_l^{\text{Tx}}\right) G_{\text{Rx}}\left(m, \phi_l^{\text{Rx}}\right) e^{j2\pi\Delta t \nu_l i},$$

where L is the total number of extracted multi-path components (MPCs), $\alpha_l, \tau_l, \phi_l^{\text{Rx}}, \phi_l^{\text{Tx}}, \nu_l$ are complex amplitude, delay, DOA
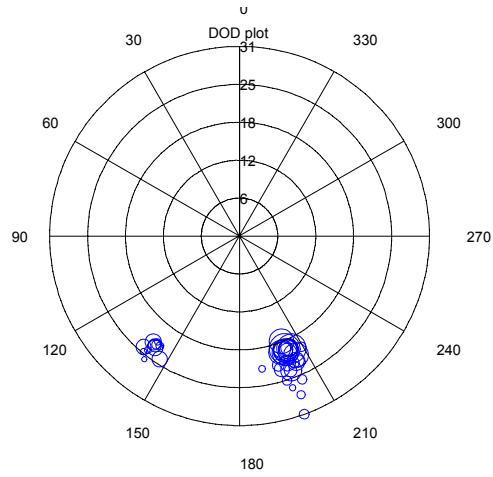

Fig. 3. DOD-delay plot for transmit position 1 with receiver in room 2336. Larger size of the circles indicate higher power of the multipath components. Radial axis in m. North in the site map corresponds to 0 degrees.

in azimuth, DOD in azimuth and Doppler frequency, respectively, of the l :th MPC. Furthermore $k, i, m, n, G_{\text{Rx}}, G_{\text{Tx}}$ are frequency sub-channel index, snapshot index, receiver element number, transmitter element number, receive (Rx) antenna pattern and transmit (Tx) antenna pattern, respectively.

All 13 snapshots were used in data processing, 40 MPCs were extracted from each measurement position using 30 SAGE iterations. We cross-checked the results with alternative high-resolution algorithms [12] and found excellent agreement of the extracted MPC parameters. It must be stressed that high-resolution algorithms based on the sum-of-plane-waves model cannot explain all possible propagation processes. For example, diffuse reflections, as well as spherical waves, are note covered by the model of Eq. (1). For this reason, the total power of the MPCs extracted by SAGE does not necessarily equal the total power of the signals observed at the antenna elements. This can be compounded by the fact that for some locations, more than 40 MPCs might carry significant energy. A quantitative discussion of this is given in Sec. IV.D.

IV. RESULTS

The estimated Doppler frequency for most MPCs was less than 1 Hz; at a few locations, Doppler frequencies of around 2-3 Hz were measured. This indicates a relatively static measurement scenario.

A. Directions of multipath components

Figs. 3-4 show the DOA–delay and DOD-delay plots for a receiver placed in room 2336, close to the northern window and with the transmit array placed at position 1 (see Fig. 2). All of the 40 extracted MPCs are plotted.

In Fig. 5 the 40 extracted MPCs are plotted for each of the 53 receiver positions, with transmitter at position 1. The received signal level is normalized for each position for clarity reasons. The length of the lines represents relative signal amplitude level on linear scale.
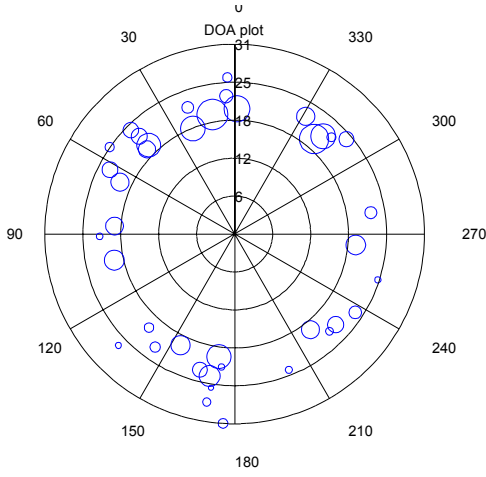
Fig. 4. DOA-delay plot for transmit position 1 with receiver in room 2336. Larger size of the circles indicate higher power of the multipath components. Radial axis in m. North in the site map corresponds to 0 degrees.
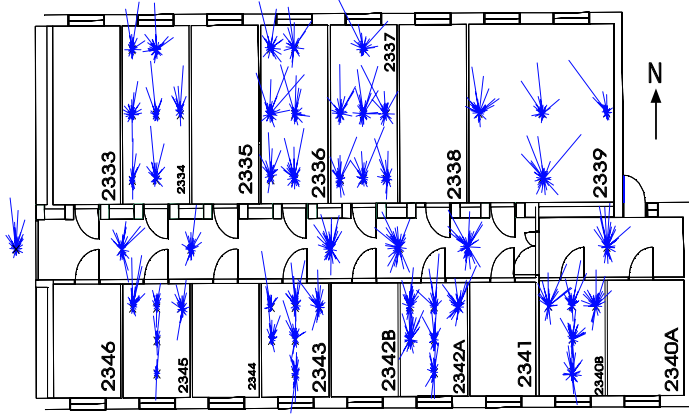

Fig. 5. DOAs at all receiver positions for transmit position 1.

This plot allows to make some important conclusions about the dominant propagation processes:

- In the northern rooms, propagation through walls and windows shows almost equal efficiency, as one can see from the (relative) strength of the LOS components in the different rooms. The reason lies in the strong attenuation by the windows as well as the walls. The (outer) walls consist of bricks, while the windows are coated with a metallic film for energy conservation. The measured attenuation for the walls is 7 dB, in excess to free space attenuation measured over the same distance, while the excess attenuation for the windows is 14 dB.
- Reflection and diffraction by the (metallic) window frames are efficient propagation mechanisms, as is evident, e.g., from the DOAs in the rooms 2334, 2336 and 2338. It is especially noteworthy that the diffraction via the the metallic frames of the windows results in an attenuation similar to the attenuation of the brick wall e.g. position west-middle in room 2336.
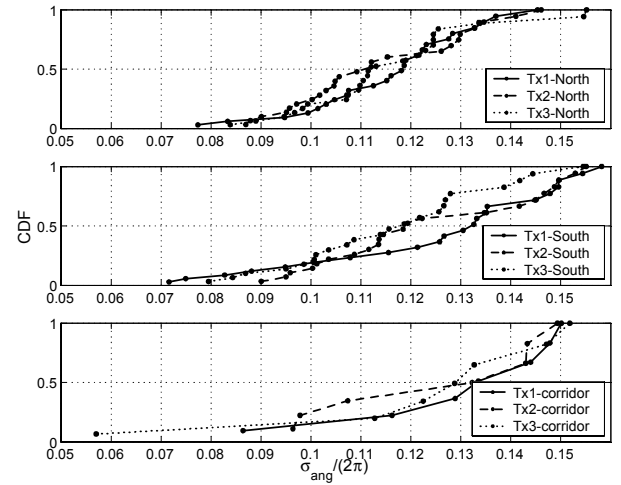- Each window has a horizontal middle section with a metal

Fig. 6. CDFs of the RMS angular spread at the receiver (DOA) for the northern and southern rooms and the corridor.

handle. Due to the metal handle there are strong MPC coming from the middle of the window e.g. the north-middle position of room 2336.
- For some southern rooms, propagation through the northern rooms, via doors, constitutes the dominant propagation mechanism. This is obvious, e.g., in the middle positions of room 2345.
- There are strong reflections coming from south in the southern rooms. These are due to over-the-rooftop propagation, combined with reflection at a building opposite of the south-facing windows (that building is similar in shape and height to the building block in Fig. 2).

For the other two transmit position, 2 and 3, similar behavior was observed.

B. RMS angular spread

The RMS angular spread is an important parameter for the characterization of spatial channel characteristics. The definition of Fleury [13] is used, which does not suffer from the ambiguity with the origin of the coordinate system:

$$\sigma_{\text{ang}} = \sqrt{\sum_{l=1}^{L} \left| e^{j\phi_l} - \mu_{\text{ang}} \right|^2 P_{\text{ang}}(\phi_l)}, \qquad (2)$$

where

$$\mu_{\text{ang}} = \sum_{l=1}^{L} e^{j\phi_l} P_{\text{ang}}(\phi_l). \qquad (3)$$

$P_{\text{ang}}(\phi_l)$ is the angular power spectrum normalized as $\sum_L P_{\text{ang}}(\phi_l) = 1$. Fig. 6 presents the cumulative distribution functions of the angular spread for different Tx and Rx locations. The differences between the northern and the southern rooms are evident, especially at the receiver side. In the corridor the RMS angular spread is close to that of the southern offices.

In Table I the mean angular spreads are presented. It is evident that the transmitter position does not affect the mean DOA
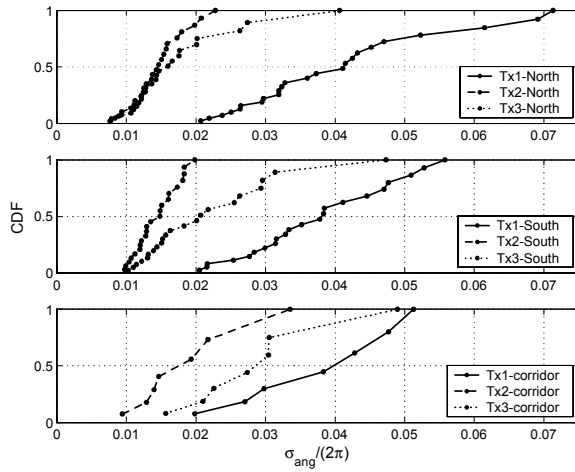
Fig. 7. CDFs of the RMS angular spread at the transmitter (DOD) for the northern and southern rooms and the corridor.

Fig. 8. CDF of the RMS delay spread for the northern and southern rooms and the corridor.

TABLE I

MEAN NORMALIZED ANGULAR SPREAD.

DOA	$\bar{\sigma}_{\mathrm{ang}}/\left(2\pi\right)$		
rooms	north	corridor	south
Tx1	0.11	0.13	0.12
Tx2	0.11	0.12	0.12
Tx3	0.11	0.12	0.11
DOD	$\bar{\sigma}_{\mathrm{ang}}/\left(2\pi\right)$		
rooms	north	corridor	south
Tx1	0.038	0.038	0.036
Tx2	0.014	0.018	0.014
Tx3	0.016	0.028	0.020

angular RMS spread, and there is no large difference in mean spread for the northern rooms, the corridor and southern rooms. However, there are large differences in the DOD spread for the different transmit positions and when comparing the mean RMS angular spread of DOA and DOD.

C. RMS delay spread

The RMS delay spread roughly characterizes the multipath propagation in the delay domain. The RMS delay spread is the square root of the second central moment of the averaged power delay profile[1] (PDP) and is defined as [14]

$$\sigma_\tau = \sqrt{\bar{\tau^2} - (\bar{\tau})^2},\qquad(4)$$

where the mean excess delay, $\bar{\tau}$, and the non-central second moment of the average PDP, $\bar{\tau^2}$, are defined to be [14]

$$\bar{\tau} = \frac{\sum_L P_{\mathrm{del}}\left(\tau_l\right)\tau_l}{\sum_L P_{\mathrm{del}}\left(\tau_l\right)} \text{ and } \bar{\tau^2} = \frac{\sum_L P_{\mathrm{del}}\left(\tau_l\right)\tau_l^2}{\sum_L P_{\mathrm{del}}\left(\tau_l\right)}.\qquad(5)$$

[1] The average power delay profile is the squared magnitude of impulse response realizations averaged over the ensemble of antenna positions at Tx and Rx.
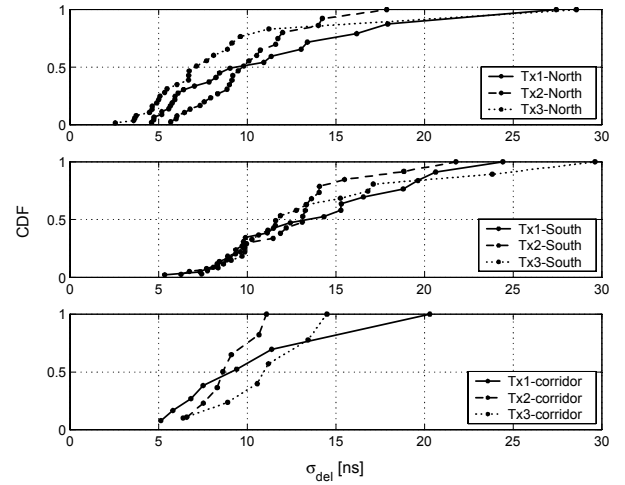
$P_{\mathrm{del}}\left(\tau_l\right)$ is the power and τ_l is the delay of the l :th MPC.

Fig. 8 presents the cumulative distribution function for the RMS delay spread in the northern and southern rooms. The delay spread has been evaluated using the MPCs as extracted from the SAGE algorithm. This has the drawback that diffuse contributions are not reflected in the obtained delay spreads (which therefore are on the low side). On the other hand, delay spread values that are extracted directly from the measured power delay profiles show much too high values, as noise contributions at large delays have a disproportionate influence. The usual technique of thresholding the PDP (for noise reduction) cannot be applied in our case, since in some cases the measurement SNRs are too low for this purpose.[2] Therefore, the delay spread values obtained from the MPC parameters were deemed more reliable.

D. Cumulative extracted power

The power captured by SAGE is dependent on, e.g., the environment and the number of extracted MPCs. The captured power as a function of the number of extracted MPCs q, compared to the received power from measured transfer matrix is defined as

$$F\left(q\right) = \frac{\left\|\hat{\mathbf{H}}\left(q\right)\right\|_F^2}{\left\|\mathbf{H}_{\mathrm{meas}}\right\|_F^2 - \hat{\sigma}_n^2}\qquad(6)$$

where $\hat{\mathbf{H}}\left(q\right)$ is the reconstructed channel matrix from the SAGE estimates and the channel model in Eq. 1. The measurement noise power estimate, $\hat{\sigma}_n^2$, at each measurement position was calculated as

$$\hat{\sigma}_n^2 = \sum_{i=1}^{I-1} \frac{\left\|\mathbf{H}_{i+1} - \mathbf{H}_i\right\|_F^2}{2\left(I-1\right)}\qquad(7)$$

where $\mathbf{H}_i$ is the measured channel transfer matrix for the i :th snapshot. The MPCs are added in descending order (of power) and not in the order detected by SAGE. In Fig. 9 the cumulative extracted power is presented at 4 receiver positions.

[2] Note that the noise problem is eliminated when evaluating the delay spread based on the MPCs, because SAGE performs an inherent noise suppression.
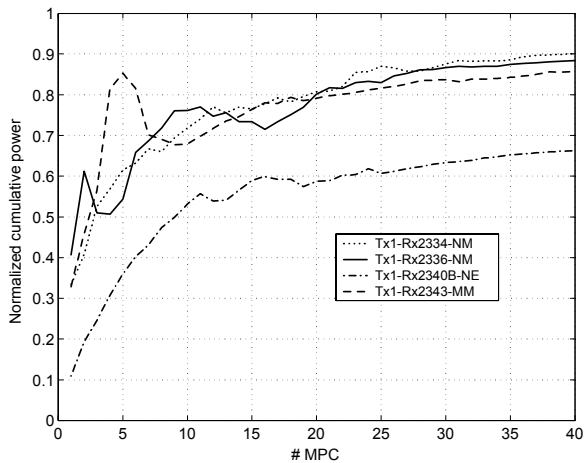
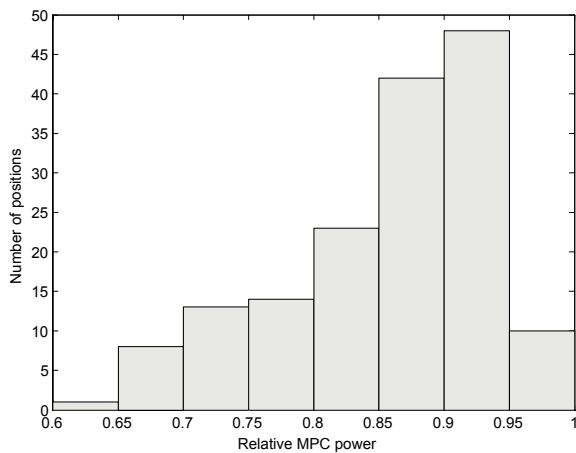Fig. 9. Normalized cumulative extracted power vs. number of estimated MPCs.

Fig. 10. Percentage of the captured power by 40 estimated MPC at the 159 measurement positions.

The non-monotonicity of the cumulative power curve is due to constructive or destructive interference when adding complex path weights of the MPCs to generate elements of the reconstructed channel matrix. The LOS scenarios capture more of the power than the non-LOS scenarios. In Fig. 10 the histogram of the power captured by 40 MPCs for all 159 locations is shown. The amount of captured power varies significantly; for some positions only about 60% of the power is captured by the 40 MPCs, but in the majority of measurements more than 85% of the power is captured.

V. Summary

In this paper we have presented the results of one of the first double-directional measurement campaigns for an outdoor to indoor office scenario. Results indicate that the angular spreads at the outdoor link end are rather small; for the indoor link end, they depend on how far the array is from the window facing the outdoor array. For the southern rooms (rooms not facing the transmitter), propagation paths are not limited to the LOS direction; MPCs of significant energy enter some of the rooms through the back window due to reflection from buildings behind the southern room.

The outdoor to indoor office wireless propagation channel was characterized, delay spread was measured to be in the range of $5 - 25$ ns. The angular spread at the indoor link end was observed to be in the range of $30 - 55$ degrees. At the outdoor link end the angular spread was in the range of $4 - 20$ degrees. By considering 40 MPC at each measured position, more than 85% of the received power could be accounted for in 60% of the 159 measurement locations.

These results form a useful basis for the design and simulation of MIMO systems with outdoor to indoor applications.

References

[1] G. J. Foschini and M. J. Gans, "On limits of wireless communications in fading environments when using multiple antennas," *Wireless Personal Communications*, vol. 6, pp. 311–335, 1998.

[2] M. Steinbauer, A. F. Molisch, and E. Bonek, "The double-directional radio channel," *IEEE Antennas and Propagation Magazine*, vol. 43, pp. 51–63, August 2001.

[3] D. Chizhik, J. Ling, P. W. Wolniansky, R. A. Valenzuela, N. Costa, and K. Huber, "Multiple-input-multiple-output measurements and modeling in Manhattan," *IEEE Journal on Selected Areas in Communications*, vol. 21, pp. 321–331, April 2003.

[4] J. Kivinen, P. Suvikunnas, L. Vuokko, and P. Vainikainen, "Experimental investigations of MIMO propagation channels," in *Proc. IEEE Antennas and Propagation Society International Symposium*, vol. 3, pp. 206–209, June 2002.

[5] R. Thoma, D. Hampicke, M. Landmann, G. Sommerkorn, and A. Richter, "MIMO measurement for double-directional channel modelling," in *Proc. IEE Seminar on MIMO: Communications Systems from Concept to Implementations (Ref. No. 2001/175) Dec. 2001*, pp. 1/1–1/7, IEE, 2001.

[6] D. McNamara, M. Beach, P. Karlsson, and P. Fletcher, "Initial characterisation of multiple-input multiple-output (MIMO) channels for space-time communication," in *Proc. IEEE Vehicular Technology Conference*, vol. 3, pp. 1193–1197, September 2000.

[7] P. Kyritsi, D. Cox, R. Valenzuela, and P. Wolniansky, "Correlation measurements of a multiple element system in an indoor environment," *IEEE Journal on Selected Areas in Communications*, vol. 21, pp. 713–720, June 2003.

[8] H. Özcelik, M. Herdin, H. Hofstetter, and E. Bonek, "A comparison of measured 8x8 MIMO systems with a popular stochastic channel model at 5.2 GHz," in *Telecommunications, ICT 2003. 10th International conference on*, vol. 2, pp. 1542–1546, 2003.

[9] J. Medbo, F. Harrysson, H.Asplund, and J. E. Berg, "Measurements and analysis of a MIMO macrocell outdoor-indoor scenario at 1947 MHz," in *Vehicular Technology Conference*, IEEE, 2004.

[10] H. T. Nguyen, J. B. Andersen, and G. Pedersen, "Characterisation of the indoor/outdoor to indoor MIMO radio chanel at 2.140 GHz," in *COST273 meeting, Gothenburg, Sweden*, 2004.

[11] B. H. Fleury, D. Dahlhaus, R. Heddergott, and M. Tschudin, "Wideband angle of arrival estimation using the SAGE algorithm," in *Proc. Spread Spectrum Techniques and Applications*, vol. 1, (Mainz), pp. 79–85, IEEE, September 1996.

[12] J. Medbo and J. E. Berg, "Spatio-Temporal channel characteristics at 5 GHz in a typical office environment," in *Proc. Vehicular Technology Conference, 2001.*, vol. 3, pp. 1256–1260, IEEE, October 2001.

[13] B. H. Fleury, "First- and second-order characterization of direction dispersion and space selectivity in the radio channel," *IEEE Transactions on Information Theory*, vol. 46, pp. 2027–2044, September 2000.

[14] P. A. Bello, "Characterization of randomly time-variant linear channels," *IEEE Transactions*, pp. 360–393, December 1963.

0-7803-8521-7/04/$20.00 (C) 2004 IEEE

105